Polymer
May 2019, Volume 173, Pages 158-165
https://doi.org/10.1016/j.polymer.2019.04.019
https://archimer.ifremer.fr/doc/00488/60003/

Strain-induced crystallization in a carbon-black filled polychloroprene rubber: kinetics and mechanical cycling

Le Gac Pierre-Yves [1, *], Albouy Pierre-Antoine [2], Sotta Paul [3]

[1] IFREMER Centre de Bretagne, Marine Structures Laboratory, BP70, 29280, Plouzané, France
[2] Laboratoire de Physique des Solides, CNRS, Université Paris-Sud, Université Paris-Saclay, 91405, Orsay, France
[3] Laboratoire Polymères et Matériaux Avancés, CNRS/Solvay UMR 5268, 87 avenue des Frères Perret, 69192, Saint-Fons, France

* Corresponding author : Pierre-Yves Le Gac, email address : pierre.yves.le.gac@ifremer.fr

Abstract :

It is shown in the present paper how the addition of a moderate amount of carbon black filler to a polychloroprene gum modifies the local strain state and alters the ability of the polymer to strain-crystallize. The study combines mechanical and X-ray diffraction performed during classical mechanical cycling and tensile impact tests. It highlights the fact that the strain modification induced by the filler addition is highly inhomogeneous: the crystallization behavior and the local draw ratio state are affected differently. The partial relaxation of the amorphous fraction by the strain-induced crystallization peviously evidenced in the pure gum is still present and should play a protective role. The effect of temperature on the crystallization correlates with the evolution of stress-strain curves. In particular the role of crystallization in stress-hardening is apparently amplified by the presence of the filler. Preliminary tensile tests reveal a drastic decrease of the induction time necessary for crystallization to develop. This implies a strain amplification effect higher than predicted from mechanical cycling analysis. It is proposed that carbon black particles have no time to relax during the fast stretching period. All these observations point to a synergistic effect between filler addition and strain-induced crystallization.

Graphical abstract

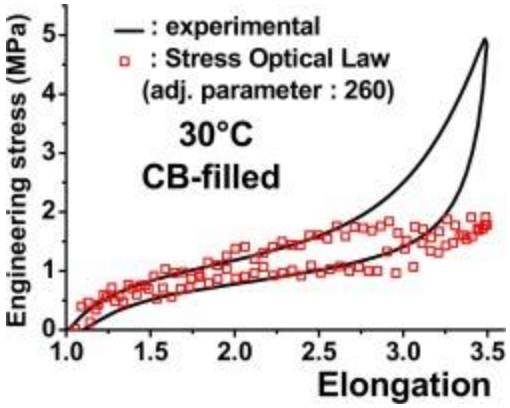

Highlights

► The effect of filler addition on SIC in polychloroprene rubber is investigated. ► Strain and stress amplification effects linked to filler addition in absence of SIC are quantified. ► SIC-related stress hardening during tensile test appears amplified by the presence of the filler. ► SIC follows a logarithmic time-dependence and develops at shorter times compared to the unfilled case.

Keywords : Polychloroprene, Strain-induced crystallization, X-ray

1. Introduction

Chloroprene rubbers (CRs) are a class of specialty elastomers widely used in many demanding industrial applications due to their good weather resistance, flame-retardant behavior and low sensitivity to swelling by nonpolar solvents and to oxidation [1]. CRs are prone to strain-induced crystallization (SIC), a phenomenon that is known to improve the mechanical properties of the material [2]. However the role of SIC has been the object of significantly fewer investigations in this class of material compared to natural rubber (NR), probably as a reflection of their respective industrial weight [3,4,5]. We recently published a detailed study of SIC in an unfilled CR material, based on simultaneous X-ray diffraction and mechanical measurements and where both mechanical cycling behavior and crystallization kinetics were investigated [6]. However CRs are most often compounded with fillers like carbon black (CB), silica or metal oxides [7,8,9]. Multi-wall carbon nanotubes or nanoclays have also been tested [10,11]. The main role of the filler is to further improve the mechanical properties and wear resistance of the material. The present study is a first step to quantify how adding CB modifies the SIC process and how this correlates with changes in the mechanical properties of the material. A low CB content was chosen so as to limit the amplitude of induced modifications and to allow an easier correlation of properties between filled and unfilled material.

The first section details the material formulation, and includes a careful characterization of its cross-link network by Multiple Quantum NMR. The X-ray set-up and the data treatment have been thoroughly described elsewhere and only relevant details are recalled here [6,12]. The experimental results are presented in the following section. Mechanical cycling is discussed first and it is shown that a single strain amplification effect cannot explain differences between filled and unfilled materials: the SIC behavior and the average local strain experienced by the amorphous matrix are affected differently. Considering the stress optical law reveals the distinction between strain and stress amplification effects. Finally the SIC-induced stress reinforcement is quantified at various temperatures. This is followed by a very preliminary study of the crystallization kinetics during tensile tests. The most impressive result is an apparent drastic decrease of the induction time for crystallization onset in the filled material compared to the unfilled one, for similar test conditions. It indicates local strains at step-end higher than expected from previously described strain amplification effects.

2. Experimental section

2.1. Materials

The polychloroprene gum is a W-type homopolymer similar to the one used in our previous study (92% *trans*-1,4 units and 4% *cis*-1,4 units). Except for the addition of 15 phr of carbon black, the formulation and vulcanization process are also identical to those previously used [6]. Samples are 20mm in length, 7mm in width and 0.5mm in thickness with cylindrical extremities. Cross-link densities for unfilled and CB-filled samples were compared using MQ-NMR [13,14]. In brief, this technique is based on the incomplete motional averaging of the movement of network chain segments fluctuating rapidly between topological constraints (cross-links or chain entanglements) compared to uncoupled segments belonging to dangling

or sol chains, or loops (i.e network defects). In the MQ-NMR procedure proposed by K. Saalwächter, a double-quantum (DQ) NMR signal is obtained together with a reference signal [15]. While the DQ signal $I_{DQ}(t)$ is due only to protons belonging to chain segments with restricted fluctuations, i.e. belonging to elastically active chains, the reference signal $I_{Ref}(t)$ contains the contributions from all protons in the material, including so-called defects, i.e. the fraction of the material which is not elastically active. The reference signal is thus the sum of two components with different time-behaviors. The signal from network defects $I_{Def}(t)$ shows a slower exponential decay and is best adjusted by a double-exponential $A_1\exp(-t/\tau_1) + A_2\exp(-t/\tau_2)$. The quantity $\varphi_{defects} = A_1 + A_2$ gives the total amount of defects. Coupled segments relax faster and non-exponentially. The normalized DQ signal is then obtained by dividing the measured DQ signal by the sum $I_{DQ}(t) + I_{Ref}(t) - I_{Def}(t)$. This signal can be adjusted by the heuristic function $\frac{1}{2}\left[1 - exp\left(-(\mathrm{D}_{res}t)^{p}\right)\right]$ where D_{res} is the residual dipolar coupling and p a shape parameter. D_{res} is shown to be proportional to the cross-link density of the material and p is qualitatively indicative of the homogeneity of the crosslink density: it lies typically between 1 and 2 and the closer its value to 1, the less homogenous is the sample. Experiments have been performed at 333K, well above Tg ≈ 228K [16] to insure fast motions and proper time averaging of spin interactions. The different parameters determined from the analysis of the DQ-NMR signals are collected in Table 1 for the filled and unfilled materials. D_{res} is 10% higher for the CB-filled samples compared to the unfilled samples. Although this difference is close to the experimental resolution, it is accordingly assumed that the cross-link density is 10% higher in the CB-filled material. Values found for the fraction of uncoupled chain segments (loops, dangling chains, sol fraction) $\varphi_{defects}$ are typical for chemically crosslinked elastomers. The shape parameters p are very close to each other, which indicates a similar degree of homogeneity of the crosslink density for both types. The cross-link density ν for the unfilled samples was estimated from mechanical measurements as previously done [6]. A higher number of tested samples and a better assessment of their geometry provided a more reliable determination $\nu = 0.802\ 10^4$ mol/cm^3, 7% higher than the previous evaluation [6]. It corresponds to an average number of 173 monomers per chain. According to this determination, the quantitative relationship between D_{res} and ν may be written:

$$\nu = 0.487 \times 10^{-4}\, D_{res}$$

With ν in mol.cm^{-3} and D_{res} in kHz, or equivalently, in terms of the average chain molecular mass between crosslinks M_c, assuming that $\nu = {}^{2\rho}/_{M_c}$ for tetrafunctional crosslinks:

$$M_c = \frac{10.25}{D_{res}}$$

With M_c in kg.mol^{-1} and D_{res} in kHz.

The Mooney-Rivlin constants ratio C_2/C_1 is unchanged and equal to 2. CB-filled samples were systematically pre-extended a few times up to the anticipated maximal extension to suppress the Mullins effect and briefly heated at 60°C to remove any trace of crystallization. All measurements were repeated on a minimum number of two samples and the actual number of investigated samples in each case is indicated in the figure captions.

Sample	D_{res} (ms^{-1})	p	$\varphi_{defects}$
Unfilled	1.6475	1.3844	4.4%
CB-filled	1.8248	1.3323	5.7%

Table 1. Parameters used to adjust the MQ-NMR signal for the two investigated materials.

2.2. Stretching set-up and data processing

The tensile machine has been described in detail elsewhere [6,12]. It is basically a symmetric stretching set-up mounted on a rotating anode generator and presently equipped with a hybrid pixel X-ray camera. Besides mechanical cycling, kinetic measurements are possible. In that case, samples are stretched to their final extension by pneumatic springs that ensure a transient stretching duration of ca.10ms.

A representative X-ray diffraction pattern of a partially strain-crystallized CB filled sample is displayed in Figure 1. Parameters pertinent to the crystalline and amorphous phases are retrieved from angular scans that encompass the area delimited by the white dotted circles. Diffuse horizontal lines in the azimuthal regions (indicated by white arrows) originate from the (001) diffraction peaks of the crystalline phase [6]. Their diffuse character is due to a chemical disorder within crystallites linked to the presence of *cis*-defects in the chains and that blurrs higher *l*-index reflections. Their detrimential effect is to limit the angular range of the scan to ± 45° when measuring the amorphous phase orientation beyond the onset of SIC.

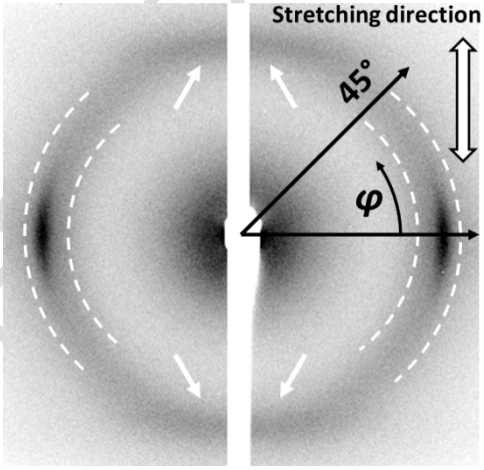

Figure 1. Representative diffraction pattern of a partially strain-crystallized CB-filled CR sample (draw ratio: 3.5; 0°C; exposure time: 10s). The blind central vertical line corresponds to the gap between the two detecting elements of the X-ray camera.

Due to the uniaxiality of the problem, the amorphous background intensity *I(φ)* can be expanded in even power of $\cos\varphi$. It remains weakly modulated and the development is stopped to the second order: $I(\varphi) = A + Bcos^2\varphi$ function. Air scattering and CB diffraction both contribute to *A*. The air scattering contribution depends upon the fraction of beam intensity transmitted

through the sample and hence upon extension. Its precise evaluation has been described elsewhere [12]. The CB contribution is evaluated from a comparison of radial diffraction scans for pure CB, and for filled and unfilled CR in the relaxed state. It is found to contribute ca. 4.6% to A and this holds at all extension states. The corrected intensity for the amorphous background $A_{Corr} + Bcos^2\varphi$ may be rewritten as a Legendre polynomial expansion to the second order $I_0 \left(1 + 5\langle P_2^{RX}\rangle (3cos^2\varphi - 1)/2\right)$. It is admitted that $\langle P_2^{RX}\rangle$ is proportional to the second Hermans coefficient $\langle P_2\rangle$ that quantifies the segmental orientation within the amorphous phase [17]. It should be noted that the precision in the determination of $\langle P_2^{RX}\rangle$ is presently significantly affected by the limited angular range of the φ-scan.

The crystalline peak is adjusted by a Pearson VII function, which is a lorentzian function raised to a power μ; this peak-function is often used in crystallography due to its versatility [18]. Physically the peak shape reflects the orientation distribution of crystallites with respect to the stretching axis. In order to limit the number of adjustable parameters the exponent μ is given a fixed value. For this purpose, the exact peak shape is retrieved from scans performed on highly crystallized samples after careful elimination of the underlying amorphous background (evaluated from scans performed on each side of the peak). This lead to an average $\mu \approx 2$ over five tests, similar to the value determined for the unfilled compound [6]. For comparison μ is found close to 5 in NR that corresponds to a nearly gaussian peak shape [12]. Lower μ–values imply a higher spread in crystallite orientation and result in more extended peak wings: it may interfere in some cases with the evalutation of the amorphous contribution during the fitting procedure and lead to a less accurate definition of $\langle P_2^{RX}\rangle$.

3. Results and Discussion

3.1. Mechanical cycling

Stress-strain curves have been recorded at a drawing speed of 6mm/min (strain-rate 5 10^{-3} s^{-1}) and the imposed maximal extension is 3.5. A temperature range 0°C-60°C has been explored by steps of 10°C. Diffraction patterns are continuously recorded with an exposure time of 10s per frame plus ca. 0.3s for the data transfer.

3.1.1. Impact of the carbon black filler

We first reveal the impact of filler addition by comparing data acquired at room temperature (20°C) for filled and unfilled samples. A direct comparison appears justified, as both materials have similar cross-link densities. We first discuss two parameters directly related to the crystallization process, the crystallinity index and the crystalline diffraction peak half-width at half-maximum (HWHM) that refers to the degree of crystallite orientation with respect to the stretching axis.

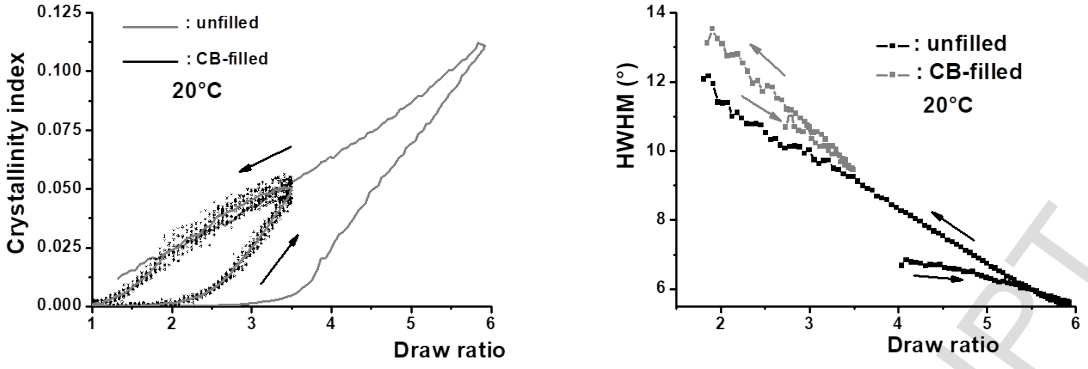

-A- -B-

Figure 2. Comparison for CB-filled and unfilled samples of the draw ratio -dependence of A- the crystallinity index; the solid gray line on top of experimental points for the CB-filled material visualizes the average over the 13 studied samples (black points). B- the half-width at half-maximum for the crystalline diffraction peak.

The SIC behavior is first addressed in Figure 2-A. A striking feature is the shift to lower draw ratios by an amount $\Delta\lambda \approx 1$ for the draw ratio at crystallization onset compared to the unfilled case. Shifts are similarly observed in natural rubber upon addition of various fillers like CB, silica, graphene sheets or carbon nanotubes and they are attributed to strain-amplification by the filler [19,20,21]. One such effect is that the strain state of the soft amorphous fraction is macroscopically enhanced due to the fact that the filler phase is rigid (see section 3.1.3). More significant for SIC is that regions located between filler particles can be submitted to local strains significantly higher than the external applied one. It should be noted that the auxiliary role of the aggregate surfaces as nucleating agent cannot be ruled out, at least for some specific fillers. We presently suppose that the shift in the crystallization onset is only due to strain-amplification by the filler, so that the elongation experienced by the gum at $\lambda \approx 2$ locally reaches ca. 3. The draw ratio-dependence of HWHM values is shown in Figure 2-B. This parameter is of primary importance: lower HWHM and hence better alignment of crystallites may help in the formation of a crystallite network we think responsible for SIC-induced stress reinforcement (see next section) [22]. For both materials, the HWHM decreases slightly during extension after crystallization onset as a consequence of the increasing orientational strain. It then increases more rapidly during unloading and we will see below that this may be related to the lower local draw ratio experienced by crystallites. Similar to what is observed in NR, the addition of CB results in a slight overall increase in the HWHM [19]. It reflects the alteration of strain distribution by the filler particles.

Representative stress-strain curves are shown in Figure 3. For both materials they are compared to the reference curves without crystallization (unfilled case: curve obtained at 50°C before SIC onset and up to sample failure; CB-filled case: extrapolated to zero-crystallinity from measurements at various temperatures, see below). SIC-induced stress reinforcement is observed for both cases during tension: its onset only becomes visible when the crystallinity index reaches typically 2% for the unfilled material, as described previously [6]. Conversely it is observed close to the crystallization onset for CB-filled materials ($\lambda \approx 2.2$). For both

compounds unloading is characterized by a rapid stress decrease as soon as the tensile motion is inverted.

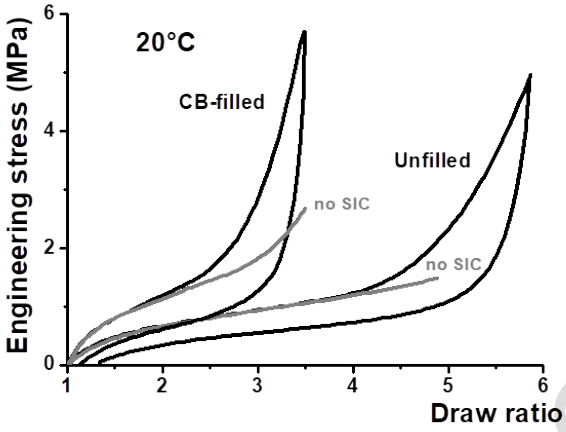

Figure 3. Stress-strain curves for CB-filled and unfilled samples.

We now turn to the local elongation of the remaining amorphous phase. In our previous work it was shown how it can be estimated from a measurement of the coefficient $\langle P_2^{RX} \rangle$ [6,21]. One significant effect of SIC that was shown for the unfilled material was a limitation of the local draw ratio, that becomes smaller than the macroscopic one; indeed we reported a similar phenomenon in natural rubber and we tentatively proposed it as one protective effect of SIC [22].

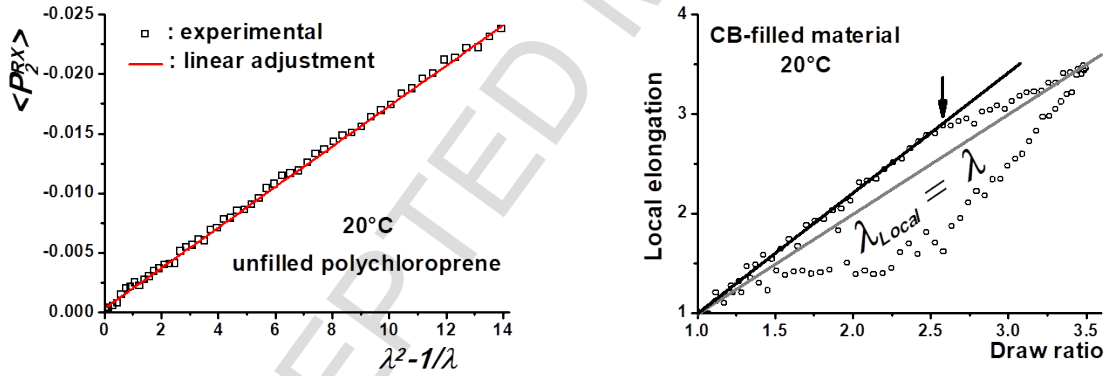

Figure 4. A- Elongation-dependence of the coefficient $\langle P_2^{RX} \rangle$ for the unfilled material before SIC onset (each point in an average over 12 samples). B- Local elongation versus applied elongation for the CB-filled material (each point in an average over 13 samples). The vertical arrow in B indicates the onset of relaxation of the local elongation.

The procedure for the determination of the local strain is now adapted to the case of the CB-filled material. A first step is the precise evaluation of the elongation-dependence of $\langle P_2^{RX} \rangle$ below SIC onset in the unfilled material. We see in Figure 4-A that it closely follows the previously reported linear dependence in $\lambda^2 - 1/\lambda$ with $\langle P_2^{RX} \rangle = -0.0017(\lambda^2 - 1/\lambda)$. This is indeed the behavior expected from the classical rubber theory in the gaussian approximation [23]. The prefactor is proportional to the cross-link density and must be thus taken 10% higher for the CB-filled material, keeping in mind that this contitutive equation will refer to the local

elongation in that case. The as-derived equation $\langle P_2^{RX}\rangle_{Filled} = -0.00187\left(\lambda_{local}^2 - {}^1/\lambda_{local}\right)$ can be inverted to yield an estimate of λ_{local} in the filled material. This is done in Figure 4-B where we see that λ_{local} depends linearly on the macroscopic draw ratio before SIC onset but with a slope ≈ 1.2 , i.e. higher than 1: this is direct evidence for a strain-amplification effect of the filler and we quantify it more precisely in the next section. The draw ratio at SIC onset $\lambda \approx 2$ is amplified to $\lambda_{local} \approx 2.2$ according to Figure 4-B, whereas a value $\lambda_{local} \approx 3$ is derived above from the actual shift of the SIC curves (see Figure 2-A). S. Dupres et al. compared strain-amplification deduced from NMR data, mechanical measurements and crystallization curves in natural rubber filled with various amounts of CB fillers [24]. They reported discrepancies between the different methods that were interpreted as an indication for some inhomgeneity of the local strain in presence of filler aggregates. Indeed the local draw ratio derived from $\langle P_2^{RX}\rangle_{Filled}$ is an average over the whole diffracting amorphous matter whereas SIC develops first in regions with higher stretching state. A marked relaxation of the local draw ratio is detected after SIC onset and for crystallinity index in excess of 1% (black arrow). This effect and a similar retardation with respect to SIC onset are also observed in the unfilled material [6]. It is recalled that this strain-relaxation is simply attributed to the fact that the fraction of chains embedded into the crystallites is fully extended along the stretching direction in average. As a consequence the remaining "molten" part gets partially relaxed. It is predicted by Flory's theory of SIC, but only under static conditions [25,26]. The rapid drop of the local draw ratio that starts at retraction coincides with the stress-drop clearly seen in Figure 2-B. This also results in a decrease of the strain-field that orientates crystallites and explains the steady increase in HWHM observed during retraction (see Figure 2-B). A plateau is then reached at the same macroscopic draw ratio where the stress drop starts to slow down.

3.1.2. Effect of temperature

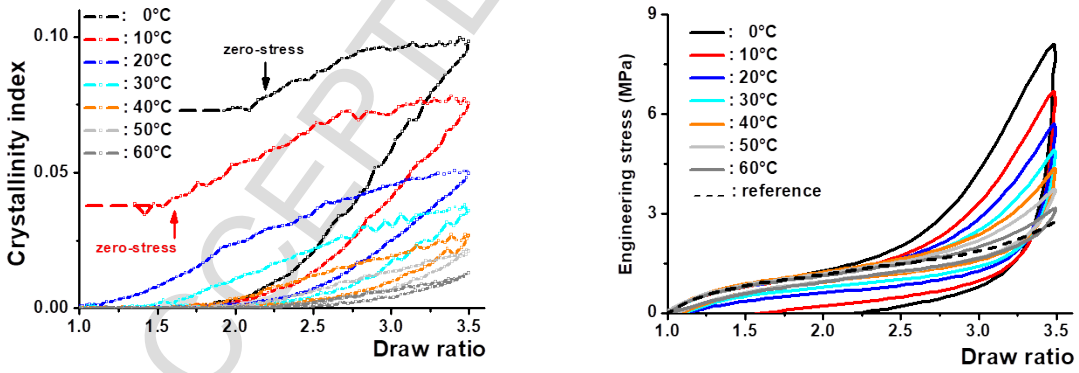

-A- -B-

Figure 5. Effect of temperature on A- the crystallinity index, B- the stress-strain curve during mechanical cycling (each curve is an average for two samples from the same batch).

The influence of temperature on the SIC process is now addressed. We see in Figure 5-A that the elongation at SIC onset does not depend markedly on temperature and lies between 2 and 2.5. Conversely the crystallization rate increases rapidly with decreasing test temperature.

During the retraction phase, complete melting after cycle completion is only observed at 20°C and above. Indeed the SIC-induced crystalline phase was shown to be partially stable below ca.17°C in the unfilled sample [6]. At 0°C and 10°C, the sample starts to bend after a zero-stress situation is reached (see Figure 5-B). At this point it is not possible to measure the crystallinity index any longer due to the sample buckling but this index is expected to remain constant (see visualization by the dashed horizontal lines in Figure 5-A). Buckling is also a macroscopic evidence that, while SIC corresponds to relaxation of the amorphous phase orientation, the crystalline phase effectively corresponds to a larger draw ratio. Moderate heating is sufficient to melt the residual crystallites and produce immediate retraction and recovery of the initial shape.

The impact of SIC on stress, already demonstrated in Figure 3, is shown strongly temperature-dependent in Figure 5-B. The dashed line is the reference curve in absence of SIC and its determination deserves some comments. It cannot be obtained experimentally as the high drawing speed and temperatures necessary to prevent SIC result in premature breakage. At a given draw ratio, the stress level and the crystallinity index are known for the different temperatures. The corresponding stress at zero-crystallization is then obtained by linear extrapolation. It is to notice that no sizeable effect of temperature is detected below SIC onset during tension. Stress is expected to increase with temperature due to its entropic origin but this effect is probably counterbalanced by the decrease of the viscosity of the amorphous fraction with temperature. Comparison between the two figures shows that stress and crystallization hysteresis correlate well. A precise quantification of the stress amplification linked to SIC is given below. As mentioned above, we see that the stress goes to zero before the end of the cycle at 0°C and 10°C as a consequence of the stability of some percentage of crystalline phase in the relaxed state.

We now turn to the local draw ratio whose behavior is illustrated in Figure 6 for the two extreme temperatures 0°C and 60°C. Similar to what is observed at room temperature (see Figure 4-B), the local draw ratio is found to be higher than the one applied before SIC onset because of filler-induced strain amplification. A very marked relaxation is observed at 0°C after SIC where the local draw ratio almost stops increasing (Figure 6-A). This is due to the rapid and massive crystallization process that occurs at this temperature (see Figure 5-A). On the contrary the SIC impact is hardly noticeable at 60°C as the crystalline content remains very small. The local draw ratio decreases rapidly upon retraction at 0°C and goes to zero for an applied elongation of ca. 2.8. This is significantly higher than the value observed for zero-stress, ca. 2.2 (see Figure 5-B), but this discrepancy is due to limited precision of the adjustment: the lower the temperature the higher the peak HWHM, as a consequence of a lower orientating local elongation. It follows that peak wings and diffraction by the amorphous fraction overlap more strongly, which results in a less accurate definition of $\langle P_2^{RX} \rangle_{Filled}$. A different behavior is observed at 60°C where the retraction part remains close to the traction one. This is again due to the very limited extent of crystallization.

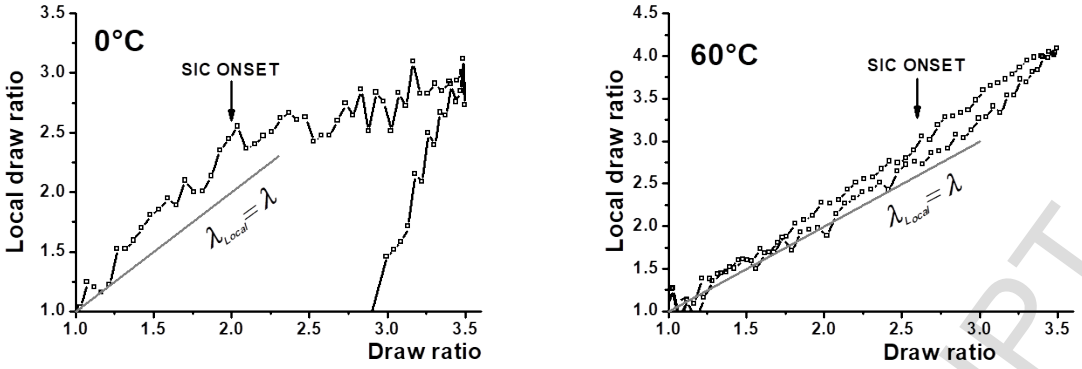

Figure 6. A- Elongation-dependence of the local draw ratio for two representative temperatures.

Curves of the local draw ratio prior to SIC onset for all investigated temperatures are collected in Figure 7. They clearly superpose for all temperatures, and display a linear dependence upon applied draw ratio.

3.1.3. Strain and stress amplification factors.

It is generally admitted that the strain amplification factor is $a_{Strain} = 1/(1-\varphi)$ where φ is the volume-fraction of non-deformable material, which includes the filler itself and the so-called occluded rubber [27]. The equation may be rewritten $\lambda_{Local} = (\lambda-\varphi)/(1-\varphi)$ and the linear adjustment represented by the heavy black line in Figure 7 with a slope ≈ 1.2 corresponds to φ = 0.18. The densities of polychloroprene and carbon black are respectively 1.23 g/cm^3 and ca. 1.7 g/cm^3 that yield an estimated carbon black volume fraction of 0.11. The difference can be attributed to occluded matrix and perhaps to a layer of immobilized rubber at the surface of the fillers, though the strain-amplification formula is certainly a simplification of reality.

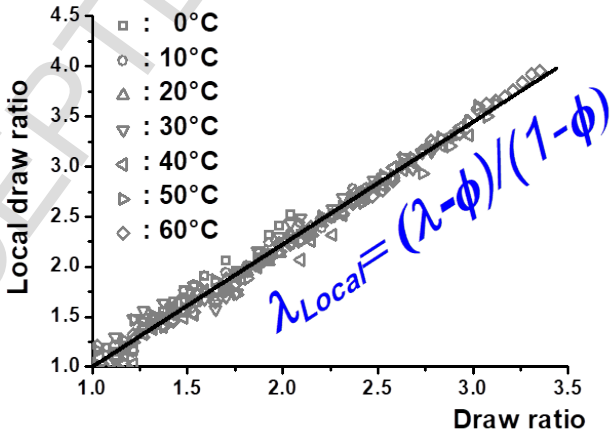

Figure 7. Draw ratio -dependence for the local draw ratio before SIC onset as measured on the tested temperature range. Each data point is an average for a minimum of two samples from the same batch.

Classical hydrodynamic theories of reinforcement of elastomers by fillers are derived from the early work by Einstein on the viscosity of a suspension of hard spheres. They notably introduce

a reinforcement factor $A(\varphi)$ defined as the ratio of the shear modulus of the filled elastomer to the one of the soft matrix in the form $A(\varphi) = 1 + 2.5\varphi + c\varphi^2$ where the quadratic term accounts for filler particle interactions and the factor *c* is usually taken equal to 14.1 [27,28,29]. The formula above results from two contributions, the strain-amplification factor a_{Strain} already introduced, and the stress amplification factor a_{Stress} that accounts for the counter-reaction of filler particles to the gum flow with $A(\varphi) = a_{Strain}^2 . a_{Stress}$. Inoue et al. recently published a paper on silica-filled SBR rubbers intended to differentiate both factors [28]. It is based on rheo-optical measurements and on the stress optical law that states that the intrinsic birefringence, or similarly $\langle P_2 \rangle$ is proportional to the deviatoric stress in a polymeric liquid (polymer solution or melt). It is expected to hold in the Gaussian regime as long as the microscopic origin of stress is chain segment orientation [30]. Indeed we also made use of this law in previous publications with the assumption that $\langle P_2^{RX} \rangle$ is proportional to $\langle P_2 \rangle$ [6,22,31]. Along these lines the entropic contribution to the engineering stress is written $-K\langle P_2^{RX} \rangle/\lambda$ where the factor $1/\lambda$ accounts for the change of the sample cross-section and the sign minus is added so as to keep *K* positive. An adjustment of the experimental engineering stress by this formula for the unfilled case is proposed in Figure 8-A with *K* = 184. It is to notice that the prediction by the stress optical law is slightly below the actual values at lower draw ratios, close to the behavior predicted in absence of Mooney-Rivlin correction. We previously observed a similar effect in natural rubber, and it was tentatively proposed that part of the Mooney-Rivlin correction is enthalpic and not entropic in nature [31].

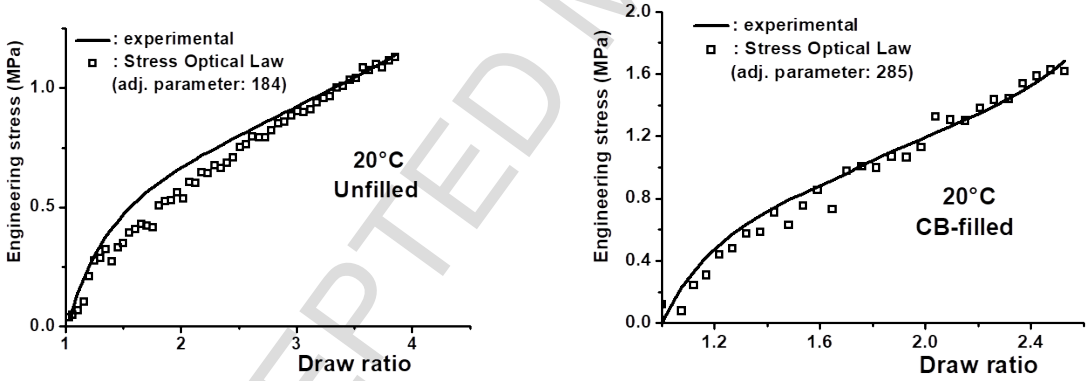

-A- -B-

Figure 8. Adjustment of the engineering stress before SIC onset by the stress optical law for A- the unfilled material, B- The CB-filled material.

It can be stated that the macroscopic true stress for the filled material σ^* is related to the true stress σ for the fraction of soft phase by the relation $\sigma^* = a_{Stress} a_{Strain} \sigma$ [27]. We make use of this formula for the present case and we write $\sigma = -K\langle P_2^{RX} \rangle_{Filled}$ considering only the entropic contribution to the stress. The engineering stress for the CB-filled material is adjusted in Figure 8-B by $-a_{Stress} a_{Strain} K\langle P_2^{RX} \rangle_{Filled}/\lambda$ with $a_{Stress} a_{Strain} \approx 1.55$. It corresponds to $a_{Stress} \approx 1.27$, which is actually smaller than predicted by the Guth and Gold formula, i.e a_{Stress} = 1.41 (*c* = 14.1 [29]).

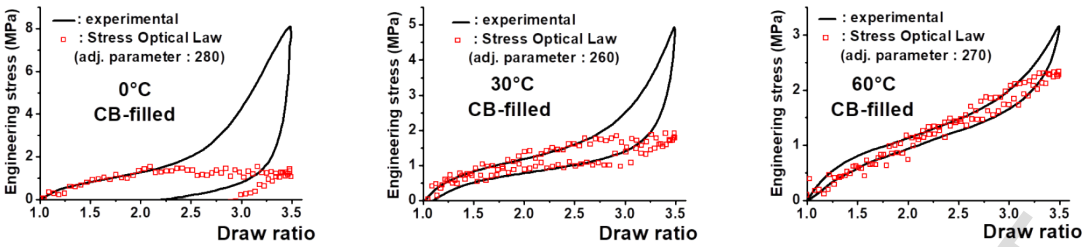

Figure 9. Contribution of the amorphous fraction to stress as derived from the stress optical law at three representative temperatures.

We conclude this paragraph by an evaluation of the reinforcement related to the SIC. For this purpose the application of the stress optical law is extended to the entire stretching range so as to evaluate the contribution to the stress from the remaining amorphous fraction [6]. Examples of adjustments obtained this way are given in Figure 9 for three representative temperatures. No significant temperature dependence is observed for the proportionality parameter which reflects the above-mentioned observation that the stress-strain curves before SIC are similar at all investigated temperatures. During stretching and after SIC onset the contribution to stress of the amorphous fraction starts to level off. During recovery and at all temperatures, the stress decreases rapidly and the amorphous contribution becomes preponderant (the derivation based on the stress optical law at 0°C goes prematurely to zero due to a poor determination of $\langle P_2^{RX} \rangle$ as explained above).

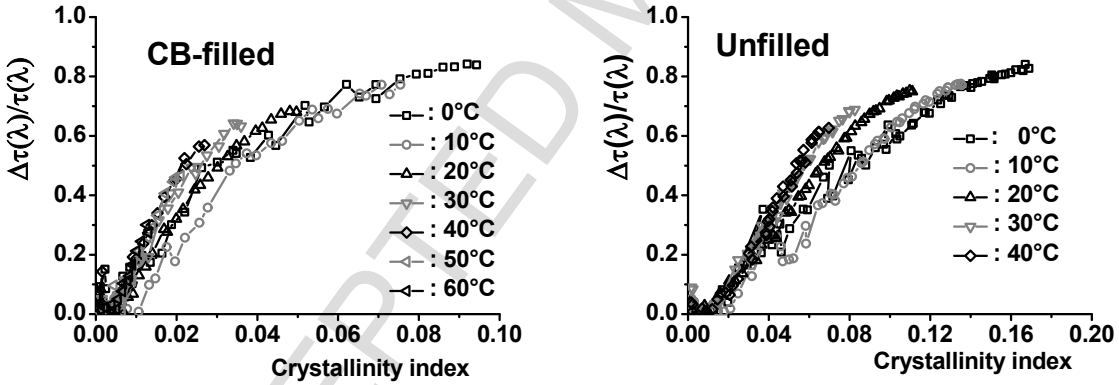

Figure 10. Contribution to the total engineering stress of the stress fraction linked to SIC.

We choose as an indicator for the SIC-induced stress change the ratio $\Delta\tau(\lambda)/\tau(\lambda)$ where $\tau(\lambda)$ is the engineering stress and $\Delta\tau(\lambda)$ the stress increment relative to the estimated contribution from the remaining amorphous fraction. This ratio is plotted in Figure 10 for both materials as a function of the crystallinity index (data for the unfilled case are derived from reference [6]). For both cases the reinforcement effect at a given crystallinity index appears more effective as the temperature is higher. We already observed this phenomenon in an unfilled NR-based material and two effects can be invoked [22]. First the alignment of crystallites improves with increasing temperature and this can facilitate their networking; however the effect is weak and the average HWHM decreases only from 11.6° at 0°C to 9.8° at 40°C. A second explanation is that crystallites formed at higher temperatures are growing under higher local strain that would

favor a higher crystallite length in the stretching direction and thus a more efficient reinforcement effect. One can further notice that SIC-induced reinforcement in presence of the filler is about twice as efficient (compare crystallinity index axis for both figures). A possible explanation is the creation of crystallite bridges between filler aggregates.

3.2. Crystallization kinetics

Some tensile impact tests have been conducted at room temperature for a unique step-end draw ratio of 3.5. Each acquisition set consists of three successive sequences of 100 diffraction frames each with exposure durations 0.3s, 3s and 30s; the data transfer time is ca. 0.3s. Measurements have been carried out on four test samples.

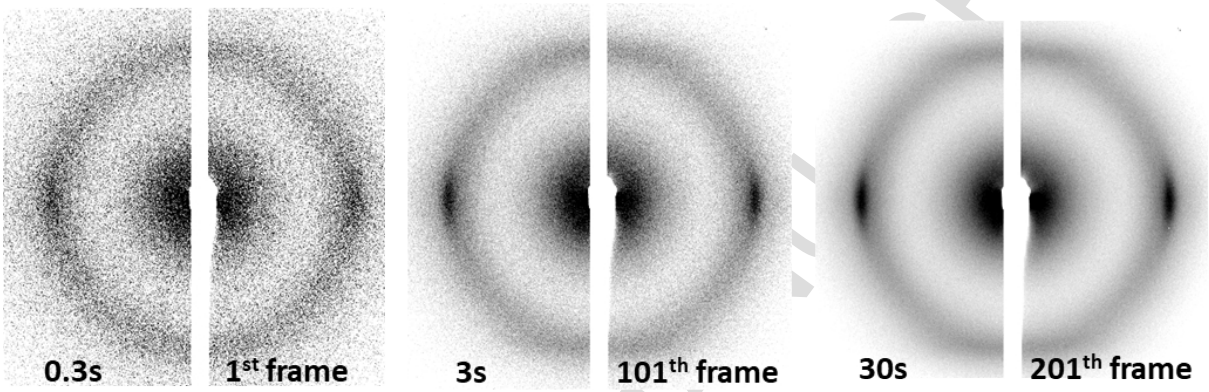

Figure 11. Diffraction patterns collected during a tensile test sequence with increasing acquisition durations (elongation at step-end: 3.5; temperature: 20°C)

Representative diffraction patterns collected during an acquisition sequence are shown in Figure 11. Reducing the exposure time to less than 0.3s would be of little benefit as transfer times are typically 0.3s. The time-dependence for the crystallinity index of all four investigated samples is displayed in Figure 12-A, and the data display a satisfactory reproducibility. Similar to the case of the unfilled material [6], a logarithmic time dependence is observed $CI(t) \approx A.log\left(t/\tau_0\right)$, where t is the elapsed time and τ_0 is tentatively interpreted as an induction time necessary for crystallization to start after step completion. In the present case, adjusted values are A = 0.00923 and $\tau_0 \approx 10^{-5}$s. It is clear that any discussion for extrapolated τ_0-values that short requires the strong hypothesis that the duration of the transient elongation step (10ms) has no significant influence. We have found in the unfilled material that the slope A is mainly dependent upon temperature and not upon draw ratio whereas τ_0 is on the contrary mainly dependent upon draw ratio and not upon temperature. We proposed the formula $A = 0.02725 - 5.2410^{-4}\vartheta\ (°C)$ for the unfilled material that gives $A \approx 0.017$ at 20°C higher than observed in the CB-filled material [6]. Similarly, the approximate relation $\tau_0 \approx 1.3\ 10^8\ exp\left(-\lambda/0.19\right)$ (seconds) proposed for the unfilled material gives a τ_0-value of the order of 1s when entering the macroscopic end- draw ratio 3.5. This is five-orders above the observed value and $\tau_0 \approx 10^{-5}$s is only reached for an draw ratio λ = 5.7 based on this formula. It points again to a strain amplification effect and this explanation is comforted by the time-dependence of the

local draw ratio derived from $\langle P_2^{RX} \rangle_{Filled}$. We see in Figure 12-B that the data are rather noisy but can be tentatively adjusted by a logarithmic time-dependence $\lambda_{local} \approx 4.04 - 0.22.log(t)$ that extrapolates to $\lambda_{local} \approx 5.1$ at 10^{-5}s. Both determinations are thus in excess of 5 and although some crystallization acceleration due to heterogeneous nucleation at the particle surface cannot be ruled out, strain-amplification appears the most significant factor. This is to compare with the value 4.1 derived from the formula $\lambda_{Local} = (\lambda - \varphi)/(1 - \varphi)$ for $\lambda = 3.5$. This is also well-above the value 4.5 that could be deduced from the shift of the elongation at crystallization onset. A possible explanation for these discrepancies is that the spatial distribution of carbon black particles has no time to reorganize during step completion so that significantly higher local strains can be attained.

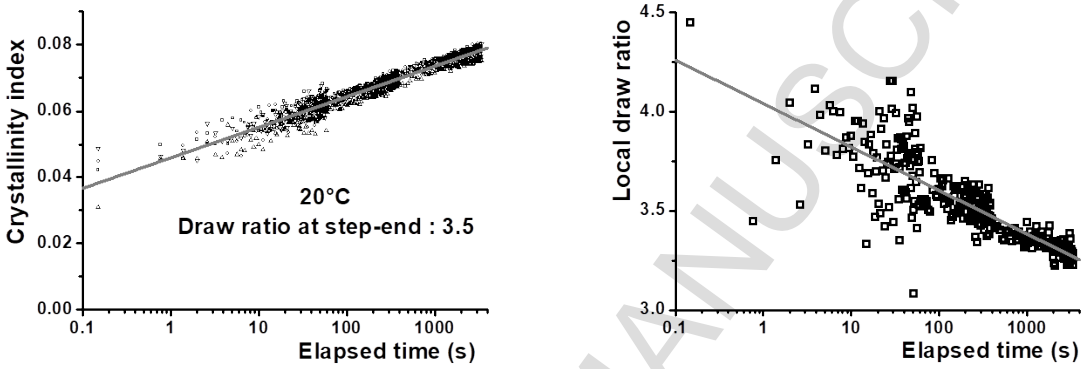

-A- -B-

Figure 12. Time-dependence of –A the crystallinity index; all four investigated samples are reported to illustrate the data dispersion; the grey line is a linear adjustment. B- the local draw ratio as computed from $\langle P_2^{RX} \rangle$. Each point corresponds to an average on the four investigated samples (20°C; elongation at step-end: 3.5).

4. Conclusion

We established how the moderate addition of carbon black filler to a W-type polychloroprene gum impacts the strain state of the amorphous fraction and alters its ability to strain-crystallize. Central to a discussion of filler effects is the notion of strain amplification. It is difficult to quantify it unequivocally as the phenomenon is most probably highly heterogeneous. Crystallization develops in the most extended region, and the as-derived local elongation is higher than the average obtained from the amorphous halo anisotropy. Inoue et al. made use of the stress optical law in silica-filled SBR rubber to separate stress and strain amplification coefficients that both contribute to the reinforcement factor [27,28]. Their method was based on dichroism measurements and it is proposed here to use X-ray diffraction with the advantage that no transparency is required. The stress amplification factor evaluated this way is found smaller than the value derived from the coefficients in the Guth and Gold formula. The stress optical law was further used to extrapolate the contribution of the remaining amorphous phase to stress beyond SIC onset. It allowed us to quantify the reinforcement due to the SIC and that we attribute to crystallite networking. It appears to be twice as efficient in presence of the filler and we tentatively attribute this increase to the establishment of crystallite bridges between

filler aggregates. Some tensile test experiments have been conducted to assess the crystallization kinetics. Similar to the unfilled case, a logarithmic time dependence is found. However the extrapolated induction time is extremely short, and points to strain amplification significantly higher than derived for mechanical cycling. Some delay for the CB-particle reorganization after draw ratio-step completion is evoked that would allow the creation of highly strained zones.

References

[1] Handbook of Elastomers, AK Bhowmick and HL. Stephens Ed., Taylor & Francis Publishers 2000.

[2] Engineering with Rubber, AN. Gent Ed. Hanser Publishers 1992.

[3] P. Zhang, G. Huang, LL. Qu, YJ. Nie, GS. Weng, JR. Wu, Strain-induced crystallization behavior of polychloroprene rubber, J. Appl. Polym. Sci. 121 (2011) 37-42.

[4] AN. Gent, Crystallization in stretched polymer networks I. trans-polychloroprene, Rubber Chem. Technol. 40 (1967) 1071-1083.

[5] B Huneau, Strain-Induced Crystallization of Natural Rubber: A Review of X-Ray Diffraction Investigations, Rubber Chem. Technol. 84 (2011) 425-452.

[6] P-Y. Le Gac, P-A. Albouy, D.Petermann, Strain-induced crystallization in an unfilled polychloroprene rubber: kinetics and mechanical cycling, Polymer 142 (2018) 209-217.

[7] BP. Holownia, Effect of carbon black on Poisson's ratio of elastomers, Rubber Chem. Technol. 48 (2975) 246-253.

[8] ST.Tchalla, P-Y. Le Gac, R. Maurin, R. Créac'hcadec, Polychloroprene behaviour in marine environment: Role of silica fillers, Polym. Degrad. Stabil., 139 (2017) 28-37.

[9] Y. Chokanandsombat, C. Sirisinha, MgO and Zno as reinforcing fillers in cured polychloroprene rubber, J. Appl. Polym. Sci. 128 (2013) 2533-2540.

[10] K. Sunbramanian, A. Das, D. Steinhauser, M. Klüpplel, G. Heinrich, Effect of ionic liquid on dielectric, mechanical and dynamic mechanical properties of multi-walled carbon nanotubes/polychloroprene rubber composites, Eur. Polym. J. 47 (2011) 2234-2243.

[11] A. Das, FR. Costa, U. Wagenknecht, G. Heinrich, Nanocomposites based on chloroprene rubber: effect of chemical nature and organic modification of nanoclay on the vulcanizate properties, Eur. Polym. J. 44 (2008) 3456-3465.

[12] P-A. Albouy, G. Guillier, D. Petermann, A. Vieyres, O. Sanseau, P. Sotta, A stroboscopic X-ray apparatus for the study of the kinetics of strain-induced crystallization in natural rubber, Polymer, 53 (2012) 3313-3324.

[13] A. Vieyres, R. Pérez-Aparicio, P-A. Albouy, O . Sanseau, K. Saalwächter, DR. Long, P. Sotta, Sulfur-cured natural rubber elastomer networks: correlating cross-link density, chain orientation and mechanical response by combined techniques, Macromolecules 46 (2013) 889-899.

[14] K. Saalwächter, A. Heuer, Chain dynamics in elastomers as investigated by proton multiple-quantum NMR, Macromolecules 39 (2006) 3291-3303.

[15] K. Saalwächter, Proton multiple-quantum NMR for the study of chain dynamics and structural constraints in polymeric soft materials, Prog. Nucl. Magn. Reson. Spectrosc. 51 (2007) 1-35.

[16] Polymer Data Handbook, JE. Mark Ed., Oxford University Press 1999.

[17] GR. Mitchell, A wide-angle X-ray study of the development of molecular orientation in crosslinked natural rubber, Polymer 25 (1984) 1562-1572.

[18] SK. Gupta, Peak decomposition using Pearson VII function, J. Appl. Cryst. 31 (1998) 474-476.

[19] S. Trabelsi, P-A. Albouy, J. Rault, Effective local deformation in stretched filled rubber, Macromolecules 36 (2003) 9093-9099.

[20] T. Spratte, J. Plagge, M. Wunde, M.Klüppel, investigation of strain-induced crystallization of carbon black and silica filled natural rubber composites based on mechanical and temperature measurements, Polymer 115 (2017) 12-20.

[21] DH. Fu, YH. Zhan, N. Yan, HS. Xia, A comparative investigation on strain induced crystallization for graphe and carbon nanotubes filled natural rubber composites, eXPRESS Polym. Lett. 9 (2015) 597-607.

[22] P-A. Albouy, A. Vieyres, R. Pérez-Aparicio, O. Sanséau, P. Sotta, The impact of strain-induced crystallization on strain during mechanical cycling of cross-linked natural rubber, Polymer 55 (2014) 4022-4031.

[23] JH. Nobbs, DI. Bower, Orientation averages for drawn rubber networks, Polymer 19 (1978)1100-1103.

[24] S. Dupres, DR. Long, P-A. Albouy, P. Sotta, Local deformation in carbon-black filled polyisoprene rubbers studied by NMR and X-ray diffraction, Macromolecules 42 (2009) 2634-2644.

[25] P. Flory, Thermodynamics of crystallization in high polymers. I crystallization induced by stretching, J. Chem. Phys. 15 (1947) 397-408.

[26] P.-A. Albouy, P. Sotta, Strain-induced crystallization in natural rubber, in ``Polymer Crystallization: from chain microstructure to processing ", Advances in Polymer Sciences, Springer, ed. by F. Auriemma, G. C. Alfonso and C. De Rosa (2016).

[27] J. Domurath, M. Saphiannikova, G. Ausias, G. Heinrich "Modelling of stress and strain amplification effects in filled polymer melts, J. Non-Newton. Fluid. 171-172 (2012) 8-16.

[28] T. Inoue, Y. Narisha, T. Katashima, S. Kawasaki, T. Tada, A rheo-optical study on reinforcement effect of silica particle filled rubber, Macromolecules 50 (2017) 8072-8082.

[29] L. Bokobza, The reinforcement of elastomeric networks by fillers, Marcomol. Mater. Eng. 289 (2004) 607-621.

[30] M. Doi, S.F. Edwards, The Theory of Polymer Dynamics; Clarendon Press: Oxford, 1995.

[31] M. Zaghdoudi, P-A. Albouy, Z. Tourki, A.Vieyres, P. Sotta, Relation between stress and segmental orientation during mechanical cycling of a natural rubber-based compound, J. Polym.Sci.Pol.Phys. 53 (2015) 943-950.